Available online at www.sciencedirect.com
ScienceDirect
Journal of Photochemistry and Photobiology A: Chemistry 197 (2008) 260–265
Journal of Photochemistry and Photobiology A:Chemistry
www.elsevier.com/locate/jphotochem

Dye-sensitized solar cells made from $BaTiO_3$-coated TiO_2 nanoporous electrodes

Li Zhang, Yunhui Shi, Shengjie Peng, Jing Liang, Zhanliang Tao, Jun Chen *

Institute of New Energy Material Chemistry and Engineering Research Center of Energy Storage and Conversion (Ministry of Education), Nankai University, Tianjin 300071, PR China

Received 10 January 2007; received in revised form 13 November 2007; accepted 5 January 2008
Available online 12 January 2008

Abstract

We reported on the preparation of a thin $BaTiO_3$-coated layer (~2.27 nm) on the surface of TiO_2 and its further application in the dye-sensitized solar cells (DSCs). The as-prepared $BaTiO_3$–TiO_2 films were characterized by X-ray diffraction (XRD), X-ray photoelectron spectroscopy (XPS), scanning electron microscopy (SEM) and transmission electron microscope (TEM). The performances of the DSCs with and without $BaTiO_3$ coating were analyzed by cyclic voltammograms (CVs), electrochemical impedance spectroscopy (EIS), and current–voltage measurements. It was found that the $BaTiO_3$–TiO_2 films with about 12 μm thickness increased the dye adsorption, resulting in increased J_{sc}. In the meantime, the $BaTiO_3$ modification on the TiO_2 surface is beneficial to the formation of an energy barrier against the electron transfer from TiO_2 to I_3^-, providing the increase of V_{oc} due to the increased electron density in the TiO_2 that is caused by the increased electron lifetime.

Keywords: Barium titanate; Titanium dioxide; Dye-sensitized solar cells; Nanoporous films

1. Introduction

Dye-sensitized solar cells (DSCs) based on nanoporous TiO_2 films have attracted great attention in the area of using clean solar energy [1]. Generally, DSCs consist of thin films of porous TiO_2 photoanode sensitized by dyes and platinum cathode with propylene carbonate containing I_3^-/I^- as an electron donor and electrolyte [2]. The porous TiO_2 electrode with large surface areas provides sufficient anchoring sites for the sensitizers to attain effective light harvesting and electron injection, resulting in the improvement of the power conversion efficiency [3,4]. However, the nanoporous TiO_2 is not perfect yet due to the close proximity of electrons and holes throughout the porous film and the absence of a substantial potential barrier at the semiconductor/electrolyte interface [5], indicating that the interfacial charge recombination still remains one of the major energy-wasting pathways [6]. It has been reported that the surface modifications of TiO_2 with oxides [7–9], metal hydroxides [10], $SrTiO_3$ [11], $CaCO_3$ [12] or organic molecules [13] could physically separate the injected electrons and the redox couple, and thereby suppressing the charge recombination reactions. Herein, we reported on the fabrication and characterization of DSCs based $BaTiO_3$-modified nanoporous TiO_2 electrodes. The results show that $BaTiO_3$ modification on the surface of TiO_2 is beneficial to the formation of an energy barrier against the electron transfer from TiO_2 to I_3^-, resulting in increased J_{sc} and V_{oc} due to the increased electron density in the TiO_2 that is caused by the increased electron lifetime.

2. Experimental

2.1. Preparation of dye-sensitized photoanode

The TiO_2 nanoporous matrix of about 12 μm thickness was fabricated on transparent conducting glass (F-doped SnO_2, 15 Ω/square, Nippon Sheet Glass Co., Japan) using a screen printing method, followed by calcinations at 450 °C for 30 min [14]. The modification of $BaTiO_3$ on the TiO_2 surface was prepared with the following steps. First, the calcinated TiO_2 thin film was dipped in the aqueous solution of saturated $Ba(NO_3)_2$ for 30 s. Second, after being washed thoroughly with water, the wet glass with the Ba^{2+} saturated

* Corresponding author.
E-mail address: chenabc@nankai.edu.cn (J. Chen).

1010-6030/$ – see front matter © 2008 Elsevier B.V. All rights reserved.
doi:10.1016/j.jphotochem.2008.01.002

TiO_2 film was sintered in air at 550 °C for 30 min. Sensitization of the $BaTiO_3$-modified TiO_2 electrode was done by overnight immersion in dry ethanol solution containing 0.3 mM of the N3 dye [*cis*-bis(thiocyanato)bis(2,2′-bipyridyl-4,4′-dicarboxylic acid)ruthenium(II)] [15].

2.2. Characterization of the modified films

The phase structure of the as-prepared films was characterized by using X-ray diffraction (XRD) of Rigaku D/max-2500 X-ray diffractometer with graphite monochromatized Cu Kα (λ = 1.5405 Å) radiation. The percentage of $BaTiO_3$ and the thickness of the coated layer were analyzed by Kratos Axis Ultra DLD multi- X-ray photoelectron spectroscopy (XPS). Field emission scanning electron microscopy (FE-SEM) images were taken using a JEOL JSM-6700F microscope. Transmission electron microscope (TEM) and high-resolution TEM (HRTEM) analyses were carried out by a Philips Tecnai F20 microscope operating at an accelerating voltage of 200 kV [16]. UV–vis absorption spectra of dye-loaded films were measured by Jasco V-550 UV–vis spectrophotometer with an integrating sphere accessory. The amount of dye adsorbed on the electrodes was estimated by measuring the light absorption in dye solution after desorption using a 0.1 M NaOH aqueous solution.

2.3. Photoelectrochemical measurements

The solar cell performance was measured in a sandwich-type configuration using Pt-coated conductive glass as a counter electrode. The composition of the electrolyte solution was dimethyl propyl imidazolium iodide (0.6 M), lithium iodide (0.1 M), iodine (0.05 M), and *tert*-butylpryidine (0.5 M) in acetonitrile. The area of the dye-adsorbed TiO_2 electrode was 0.16 cm^2. A 500 W xenon lamp in combination with a band-pass filter (400–800 nm) to remove ultraviolet and infrared radiation was served as the light source. Further calibration was carried out by a USB4000 plug-and-play miniature fiber optic spectrometer (Ocean company, USA) to give an AM 1.5 simulated sunlight so as to reduce the mismatch between the simulated and true solar spectra to less than 2%.

The applied potential and cell current were measured using a Keithley model 2400 digital source meter (Keithley, USA) [17]. The cell was operated in the short-circuit mode. The incident photon-to-current conversion efficiency (IPCE) values were determined in the range of 400–750 nm with light intensity measurement of a USB4000 instrument (Ocean Company).

The electrochemical performance was investigated by means of a PARSTAT 2273 instrument. The electrochemical impedance measurements were carried out applying bias of the open-circuit voltage, V_{oc}, namely, under the conditions of no electric current. The amplitude of the ac signal used was 10 mV, and the frequency ranged between 100 kHz and 100 mHz. The impedance spectra were characterized using Zsimpwin software. Cyclic voltammograms (CVs) were obtained at a scan rate of 0.3 V/s using a platinum wire and $Ag/AgNO_3$ as the counter and the reference electrode, respectively. $Ag/AgNO_3$ was calibrated by measuring the redox potential of ferrocene dissolved in acetonitrile/AcOH (7/1, v/v). The redox potential referenced to calibrated $Ag/AgNO_3$ was converted to the NHE (normal hydrogen electrode). Dry acetonitrile/AcOH (7/1, v/v) containing

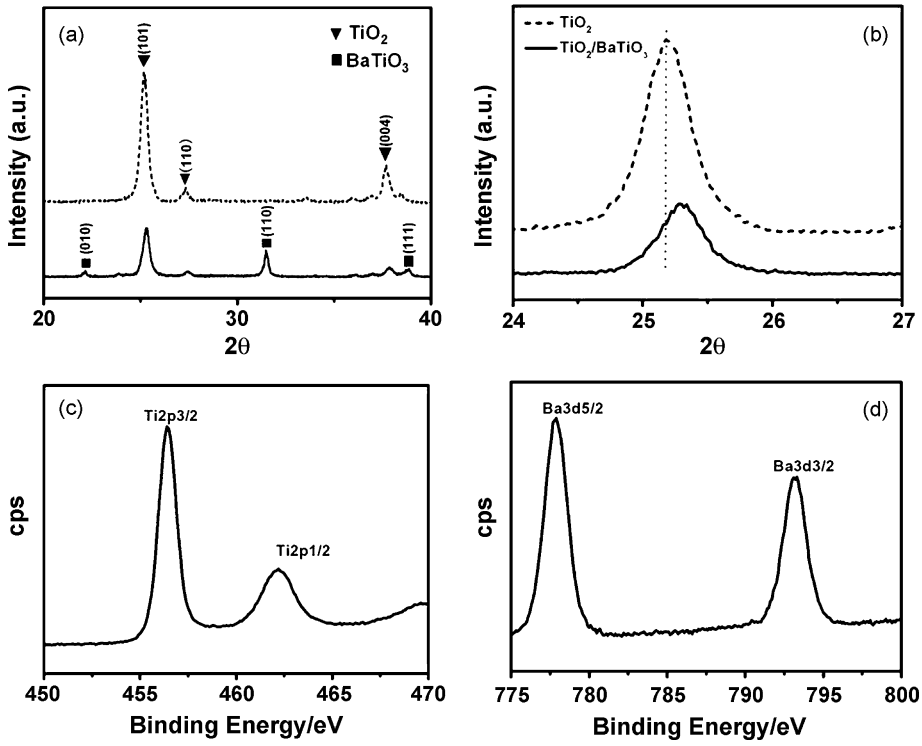

Fig. 1. XRD patterns (a and b) and high-resolution XPS spectra (c and d) of a TiO_2 film (dotted line) and after $BaTiO_3$ coating (solid line).

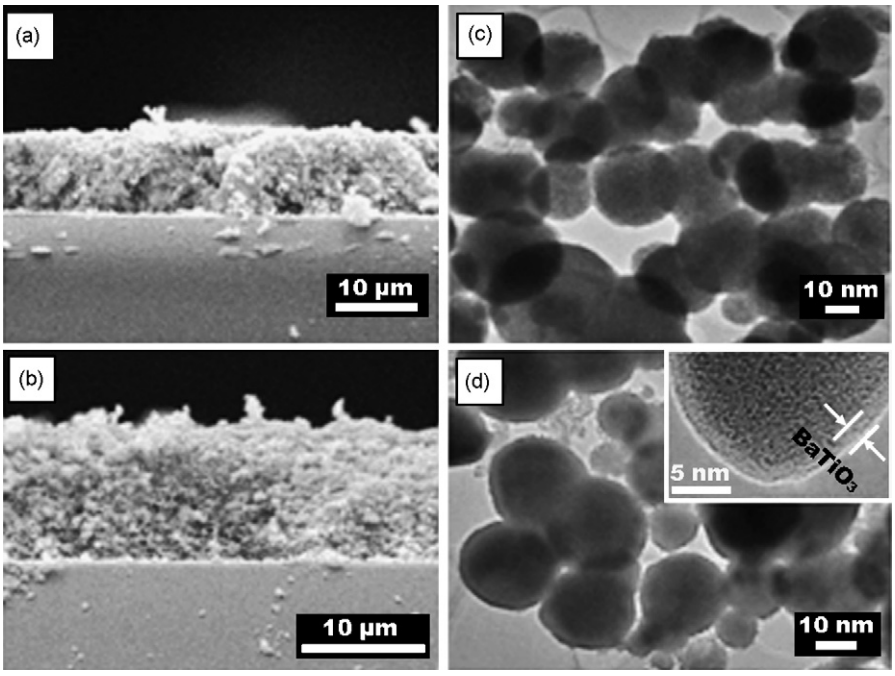

Fig. 2. Cut-through FE-SEM images of TiO_2 films without (a) and with (b) $BaTiO_3$ coating and TEM images for the particles of pure TiO_2 (c) and $BaTiO_3$-coated TiO_2 (d). The inset of (d) shows the coating of $BaTiO_3$ is about 2 nm.

0.1 M tetrabutylammonium perchlorate was used as the supporting electrolyte. To avoid oxygen, the solution was bubbled with nitrogen for 30 min before the experiments.

3. Results and discussion

Fig. 1a and b shows the XRD patterns of the TiO_2 films with and without $BaTiO_3$ modification. The XRD in Fig. 1a confirms the presence of $BaTiO_3$ on the coated TiO_2 film without any BaO or other phases. As can be seen from Fig. 1b, the diffraction peak of crystal plane (1 0 1) of pure TiO_2 shifts about 0.1° to a higher 2θ angle, which was induced by an epitaxial growth between the parallel plans in the square facet of the rutile tetragonal unit cell and the cubic unit cell of $BaTiO_3$ [18]. The unit parameters of perovskite $BaTiO_3$ closely resemble with those of rutile with the mismatch of 5%, agreeing with the lattice matching rule of epitaxial growth [19]. Thus, the appearance of (1 1 0) peak for $BaTiO_3$ at $2\theta = 31.5°$ indicates that $BaTiO_3$ grows with the parallelism of the {1 1 0} planes of rutile.

Fig. 1c and d shows XPS measurements for the TiO_2 films with and without $BaTiO_3$ modification. Peaks located at 456.4 and 462.2 eV in Fig. 1c account for titanium 2p3/2 and 2p1/2, while peaks at 777.7 and 793.2 eV in Fig. 1d can be assigned to barium 3d5/2 and 3d3/2, in agreement with the binding energies in $BaTiO_3$ reported in the literature [20]. XPS quantification shows 19.5% atomic concentration of Ba 3d. Given this molar ratio, the average thickness of $BaTiO_3$ coating layer could be estimated to be 2.27 nm. For the thickness calculation, we assumed that a homogeneous layer was deposited on the top of TiO_2. Therefore, it can be inferred from the results of XRD and XPS that a thin $BaTiO_3$ monolayer was formed on the TiO_2 surface.

Fig. 2a and b displays the FE-SEM images of the cross-section for the uncoated and $BaTiO_3$-coated TiO_2 films. The thickness of TiO_2 film in Fig. 2a is about 12 μm. Upon coating with $BaTiO_3$, the film thickness retains, but the particle assembly changes from the compact structure to the less dense porous structure (Fig. 2b). The necking growth of $BaTiO_3$ overlayer on the TiO_2 surface inhibited the aggregation of the particles during the sintering process. Fig. 2c and d shows the TEM images for the particles removed from the corresponding films. From Fig. 2c, it can be seen that the average particle sizes of the TiO_2 spheres are about 25–30 nm. The TEM image in Fig. 2d clearly demonstrates that a layer of ~2 nm thickness attributed to $BaTiO_3$ (inset in Fig. 2d) is epitaxially coated onto the surface of TiO_2 particles, verifying the above results of XRD and XPS. This coating thickness is comparable to the literature values obtained in a similar way for the conformal overlayer of Al_2O_3 (~2–2.5 nm) [21] and Nb_2O_5 (~2.7 nm) [22].

Fig. 3a presents the UV–vis absorption spectra of the dye-loaded TiO_2 films with and without $BaTiO_3$ overlayer. Since the strong TiO_2 band-gap absorption with onset at ~380 nm, which hides the interfacial charge transfer (CT) band induced by complexes from N3 dye and Ti^{4+}, shows little difference between the TiO_2 film and the modified system, we did not give the data below 400 nm. It can be seen that with $BaTiO_3$ coating, the maximum absorption peak at ~530 nm blue shifts by ~10 nm, and the maximum absorbance is enhanced. The surface concentration of the dye increased to 7.33×10^{-8} from 6.56×10^{-8} mol cm^{-2}. The higher dye concentration of N3 could be understandable by the higher basicity of TiO_2 upon $BaTiO_3$ modification. The isoelectric point of $BaTiO_3$ is ~8 [23], higher than that of TiO_2 (~5) [9], indicating that the surface of the $BaTiO_3$ coating is more basic than that of TiO_2. The carboxyl groups in the N3

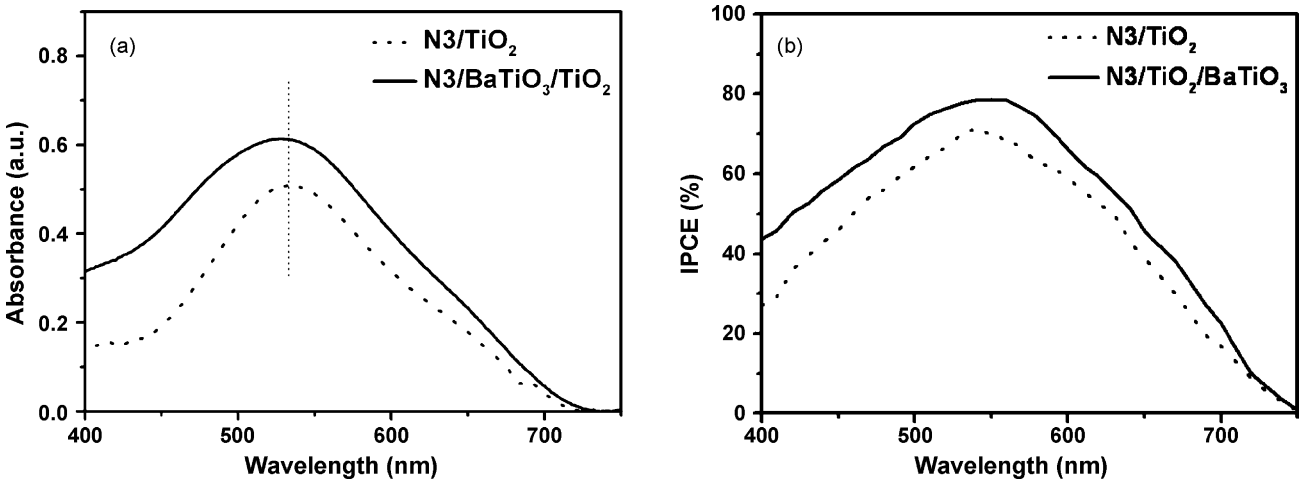

Fig. 3. Absorption spectra (a) and IPCE action spectra (b) for the dye-sensitized TiO_2 (dotted line) and $BaTiO_3$-coated TiO_2 (solid line) films.

dye molecules are more easily adsorbed to the surface of the basic coating layers [7,12,24]. It is noted that a few groups have studied the interesting effects of the acid- or base-pretreatment on the sensitized nanocrystalline TiO_2 thin films [7,8,12,24–28]. Wang et al. [26] observed that surface treatment of nanocrystalline TiO_2 films with hydrochloric acid increased the adsorbed amount of dyes as well as the short-circuit photocurrent of the corresponding solar cell. Grätzel's group reported that the dye attachment is most effective with barrier coating with high points of zero charge (basic coating) [7]. The better dye adsorption on the surface of the basic covering layer favors attachment of the dyes with carboxyl groups [8]. Similar behaviors have been also found for TiO_2 electrodes modified by $CaCO_3$, $BaCO_3$ and MgO [12,24,27]. Qu and Meyer showed that both acid- and base-pretreated samples could increase the dye surface coverage through two different binding ways [28]. High surface proton concentrations favor a "carboxylic acid" type linkage, while low proton concentrations favor "carboxylate" type binding modes. Thus, the pH-dependent interfacial property between the sensitizer and the semiconductor is relatively complicated.

Fig. 3b shows the action spectra of monochromatic incident photo-to-current conversion efficiencies (IPCEs) for the sandwiched DSCs. The $BaTiO_3$-coated TiO_2 electrode shows higher photoelectrical response than that of the bare TiO_2 electrode throughout the visible spectrum, with its maximum of 80% at 550 nm. Thus, the photon-to-current conversion efficiency was improved upon the $BaTiO_3$ surface modification, resulting in increased J_{sc}.

Fig. 4a shows the cyclic voltammograms of the two DSCs in tetrabutylammonium perchlorate acetonitrile solution. From Fig. 4a, it can be seen a gradual onset of the capacitive current in the forward scan due to the injection of the surface-trap-state electrons below the bulk conduction band edge [13]. However, the much lower capacitance is found for the $BaTiO_3$ modified system compared to that of the uncoated electrode. This implies that the number of deep trap-state electrons existing in the surface of TiO_2 [29] is decreased upon the modification of $BaTiO_3$. For the reverse scans, the current approached zero at the more positive potentials, indicating that the injected negative charge is completely recovered.

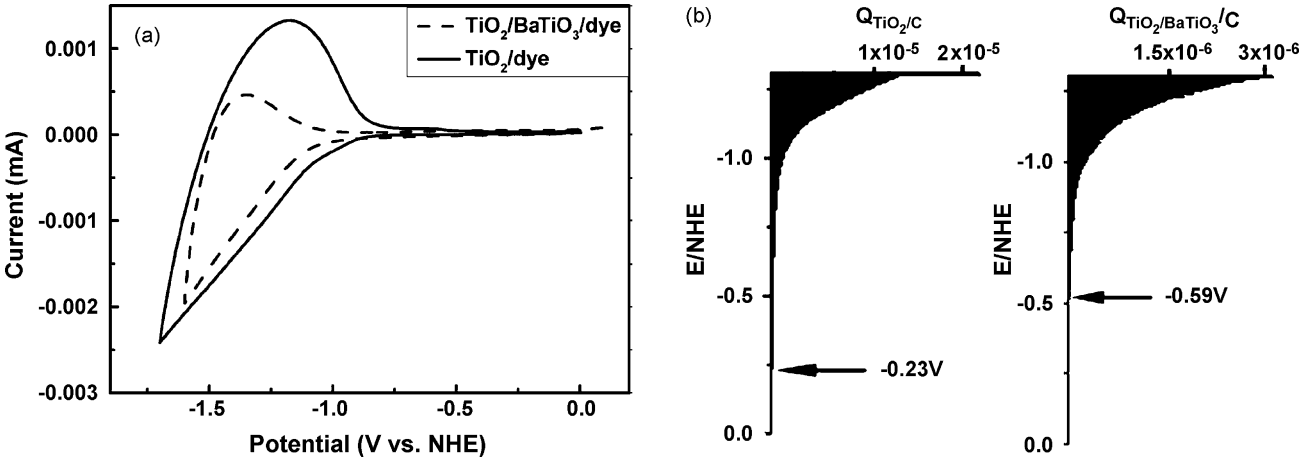

Fig. 4. (a) Cyclic voltammograms of TiO_2 electrode without (solid line) and with $BaTiO_3$ coating (dotted line) in tetrabutylammonium perchlorate acetonitrile solution. (b) Energy levels for the interfaces of mesoscopic TiO_2 and $BaTiO_3$–TiO_2 in tetrabutylammonium perchlorate.

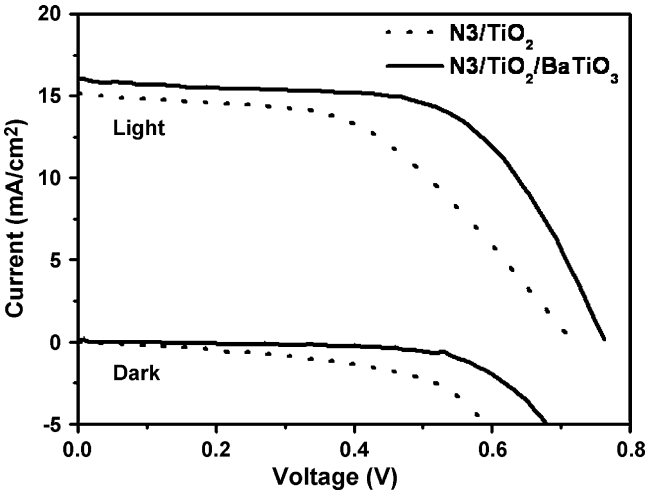

Fig. 5. Current density vs voltage (J–V) characteristics of dye-sensitized solar cells without (dotted line) and with $BaTiO_3$ coating (solid line) at 100 mW/cm^2 (AM 1.5 simulated solar illumination) and in the dark.

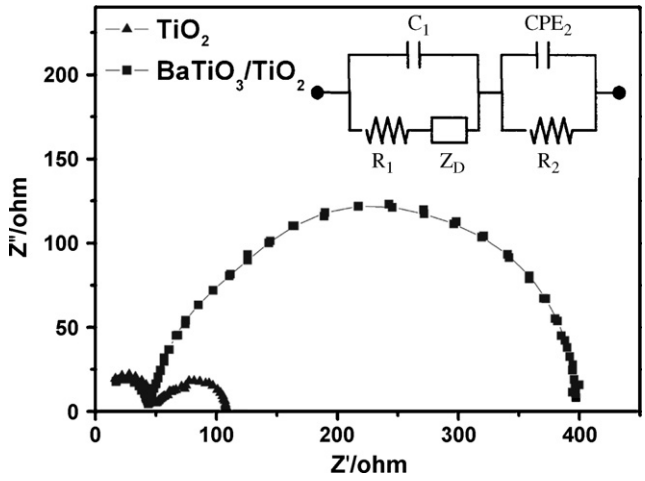

Fig. 6. Electrochemical impedance spectra of two DSCs with (■) and without $BaTiO_3$ coating (▲) measured with an external potential of −0.72 V in the dark. The inset shows the equivalent circuit, [C_1 (R_1Q_1)] (R_2Q_2), used for fitting the impedance spectra.

Since the current $I(V)$ is proportional to the differential capacity (C) in a linear sweep (constant scan rate, $dV/dt = \nu$), the energetic distribution of the acceptor state at the surface of porous photoanode can be deduced from the cyclic voltammograms via the following equation [13]

$$d(Q) = \frac{1}{\nu} I(V) dV \quad (1)$$

where Q is the total injected charge, $I(V)$ is the current, V is the potential applied on the electrode, and ν represents the constant scanning rate in the cyclic voltammetry measurements. The integration of Eq. (1) will give Q, the total number of surface states as plotted vs a function of the electrode potential (Fig. 4b). The onset is around −0.23 V (vs NHE) for the TiO_2 electrode, whereas in the case of the $BaTiO_3$-modified TiO_2 electrode, it moves to −0.59 V (vs NHE), implying that an energy barrier is most possibly formed at the electrode–electrolyte interface with the $BaTiO_3$ coating. This energy barrier could suppress the back electron-transfer process and provide a higher photo to current conversion efficiency.

Fig. 5 shows the current–voltage curves for DSCs with and without the $BaTiO_3$ coating layer. Table 1 summarizes the I–V characteristics and the conversion efficiency of the two DSCs. We can conclude that the $BaTiO_3$ coating results in an increase of all cell parameters. The open-circuit voltage (V_{oc}), the short-circuit current (J_{sc}), and the fill factor (*ff*) were increased from 716 to 766 mV, 15.12 to 16.29 mA/cm^2, and 0.5 to 0.61, respectively. As a result, the cell efficiency (η) was significantly improved from 5.46% to 7.52%. The improvement of all cell parameters should be owing to the suppression of the interfacial recombination, which results from the energetic barrier formed by the $BaTiO_3$ coating on the TiO_2 surface.

Table 1
Photovoltaic output parameters of dye-sensitized solar cells without (Device A) and with (Device B) $BaTiO_3$-coated TiO_2 layers (100 mW/cm^2, global AM 1.5)

Device	J_{sc} (mA cm^{-2})	V_{oc} (mV)	*ff*	η (%)
A	15.12	716	0.502	5.46
B	16.29	766	0.612	7.52

V_{oc} is defined as the voltage at which the photocurrent becomes zero, J_{sc} is defined as the photocurrent at zero voltage, the fill factor (*ff*) is calculated from the equation $ff = (J_{max} \times V_{max})/(J_{sc} \times V_{oc})$, and the power conversion efficiency (η) is calculated from the equation $\eta = 100\ (J_{max} \times V_{max})/P_{in}$, where P_{in} is the power of the incident light.

Fig. 6 shows typical electrochemical impedance spectra of DSCs with and without $BaTiO_3$ modification measured in the dark at an identical forward bias of −0.72 V. The Nyquist plots consist of two semicircles. The semicircle in the high-frequency region is assigned to the impedance related to charge transport at the Pt counter electrode, while the semicircle in the low-frequency region represents the electron transfer at the TiO_2/electrolyte interface. In the later case, an accumulation and recombination of electrons and the redox species are expected. Fitting the low-frequency semicircle subsequently gives charge-transfer resistance (R_{rec}) and chemical capacitance (C_μ) [30]. Comparing the results modeled by using Z-view software, it can be seen that the $BaTiO_3$-coated cell exhibits higher values for R_{rec} resistance (353.4 Ω) and lower values for the C_μ capacitance (501.38 μF cm^{-2}) than that of the uncoated cell with 58.9 Ω for R_{rec} and 786.25 μF cm^{-2} for C_μ. The similar behavior has been observed in the improved device performance by the treatment of the TiO_2 surface with proton exchange where R_{rec} increased from 37.9 to 166.4 Ω [31]. Furthermore, the response time representing the electron lifetime (τ_r) was determined according to $\tau_r = R_{rec}C_\mu$, yielding 28.27 ms for the $BaTiO_3$ modified cell. In comparison, the τ_r for the unmodified cell is 7.41 ms. These results suggest that the $BaTiO_3$ overlayer enhances the electron lifetime, thus contributing to the suppression of electron leakage and the increase of the V_{oc}.

4. Conclusions

We have demonstrated a simple sintering route to grow a $BaTiO_3$ coating layer (∼2.27 nm) on the TiO_2 surface. UV–vis

absorption spectra showed that the as-prepared $BaTiO_3$–TiO_2 film can adsorb more dyes. Under the same experimental conditions, the overall photovoltaic device efficiency for the cell made from $BaTiO_3$-coated TiO_2 electrode reached 7.52%, with a 27% enhancement compared to that of the uncoated TiO_2 electrode. The improvement of all cell parameters (J_{sc}, V_{oc}, *ff*, η) by the $BaTiO_3$ modification is owing to the formation of an energy barrier against the electron transfer from TiO_2 to I_3^- and the increased electron density in the TiO_2 caused by the increased electron lifetime.

Acknowledgments

This work was supported by the National 973 Project (2005CB623607) and Tianjin City Project (07ZCGHHZ00700).

References

[1] B. O'Regan, M. Grätzel, Nature 353 (1991) 737.
[2] (a) O. Schwarz, D. van Loyen, S. Jockusch, N.J. Turro, H. Dürr, J. Photochem. Photobiol. A: Chem. 132 (2000) 91;
(b) H. Li, B. Zhong, L. He, G. Yang, Y. Li, S. Wu, J. Liu, Appl. Phys. Lett. 80 (2002) 2299.
[3] Q. Wei, K. Hirota, K. Tajima, K. Hashimoto, Chem. Mater. 18 (2006) 5080.
[4] M. Grätzel, J. Photochem. Photobiol. A: Chem. 164 (2004) 3.
[5] A. Hagfeldt, M. Grätzel, Chem. Rev. 95 (1995) 49.
[6] G.R.A. Kumara, M. Okuya, K. Murakami, S. Kaneko, V.V. Jayaweera, K. Tennakone, J. Photochem. Photobiol. A: Chem. 164 (2004) 183.
[7] A. Kay, M. Grätzel, Chem. Mater. 14 (2002) 2930.
[8] E. Palomares, J.N. Clifford, S.A. Haque, T. Lutz, J.R. Durrant, J. Am. Chem. Soc. 125 (2003) 475.
[9] Y. Diamant, S. Chappel, S.G. Chen, O. Melamed, A. Zaban, Coordin. Chem. Rev. 248 (2004) 1271.
[10] J.H. Yum, S. Nakade, D.-Y. Kim, S. Yanagida, J. Phys. Chem. B 110 (2006) 3215.
[11] Y. Diamant, S.G. Chen, O. Melamed, A. Zaban, J. Phys. Chem. B 107 (2003) 1977.
[12] Z.S. Wang, M. Yanagida, K. Sayama, H. Sugihara, Chem. Mater. 18 (2006) 2912.
[13] Z. Zhang, S.M. Zakeeruddin, B.C. O'Regan, R. Humphry-Baker, M. Grätzel, J. Phys. Chem. B 109 (2005) 21818.
[14] M. Liang, W. Xu, F. Cai, P. Chen, B. Peng, J. Chen, Z.M. Li, J. Phys. Chem. C 111 (2007) 4465.
[15] M.K. Nazeeruddin, A. Kay, I. Rodicio, R. Humphry-Baker, E. Müller, P. Liska, N. Vlachopoulos, M. Grätzel, J. Am. Chem. Soc. 115 (1993) 6382.
[16] X. Gou, F. Cheng, Y. Shi, L. Zhang, S. Peng, J. Chen, P. Shen, J. Am. Chem. Soc. 128 (2006) 7222.
[17] F. Cai, J. Chen, R. Xu, Chem. Lett. 35 (2006) 1266.
[18] S.G. Chen, S. Chappel, Y. Diamant, A. Zaban, Chem. Mater. 13 (2001) 4629.
[19] S. Chappel, S.-G. Chen, A. Zaban, Langmuir 18 (2002) 3336.
[20] U.A. Joshi, S. Yoon, S. Baik, J.S. Lee, J. Phys. Chem. B 110 (2006) 12249.
[21] E. Palomares, J.N. Clifford, S.A. Haque, T. Lutz, J.R. Durrant, Chem. Commun. 24 (2002) 1464.
[22] A. Zaban, S.G. Chen, S. Chappela, B.A. Gregg, Chem. Commun. 22 (2000) 2231.
[23] P. Gherardi, E. Matijevic, Colloids Surf. 32 (1988) 257.
[24] X. Wu, L. Wang, F. Luo, B. Ma, C. Zhan, Y. Qiu, J. Phys. Chem. C 111 (2007) 8075.
[25] A. Zaban, S. Ferrere, B.A. Gregg, J. Phys. Chem. B 102 (1998) 452.
[26] (a) Z.S. Wang, F.Y. Li, C.H. Huang, J. Phys. Chem. B 105 (2001) 9210;
(b) Z.S. Wang, T. Yamaguchi, H. Sugihara, H. Arakawa, Langmuir 21 (2005) 4272.
[27] H.S. Jung, J.K. Lee, M. Nastasi, S.W. Lee, J.Y. Kim, J.S. Park, K.S. Hong, H. Shin, Langmuir 21 (2005) 10332.
[28] P. Qu, G.J. Meyer, Langmuir 17 (2001) 6720.
[29] Z.S. Wang, C.H. Huang, Y.Y. Huang, Y.J. Hou, P.H. Xie, B.W. Zhang, H.M. Cheng, Chem. Mater. 13 (2001) 678.
[30] C. Longo, A.F. Nogueira, M.-A.D. Paoli, H. Cachet, J. Phys. Chem. B 106 (2002) 5925.
[31] Z.S. Wang, H. Sugihara, Langmuir 22 (2006) 9718.